

Supporting Information

Optimum nanoscale design in ferrite based nanoparticles for magnetic particle hyperthermia

S. Liébana-Viñas, K. Simeonidis, U. Wiedwald, Z.-A. Li, Z. Ma, E. Myrovali, A. Makridis, D. Sakellari, G. Vourlias, M. Spasova, M. Farle and M. Angelakeris

Table S1: Magnetic features as extracted from hysteresis loops and ZFC-FC curves

MNPs system	$\mu_0 H_c^{@10\text{K}}$ (mT)	M_s (A m ² /kg)	T_B (K)*
MnFe ₂ O ₄	0.4	27	80
Fe ₃ O ₄ @MnFe ₂ O ₄	0.2	60	250
CoFe ₂ O ₄	1.8	52	230
Fe ₃ O ₄ @CoFe ₂ O ₄	1.1	73	> RT

* The blocking temperature in our case is only based on a rough estimation of a not well defined maximum in the ZFC curve. All T_B values now appear with a ± 10 -20 °C depending on the accuracy of peak position.

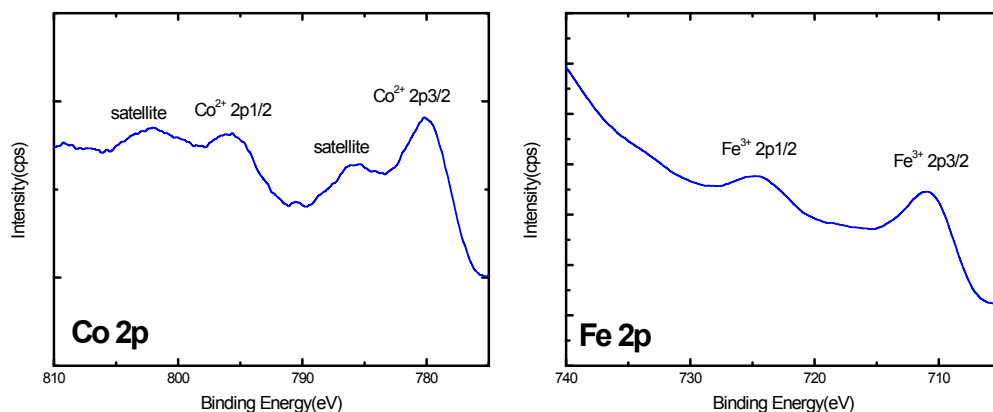


Figure S1. High resolution XPS spectra (Co 2p and Fe 2p) of CoFe₂O₄ nanoparticles. The Co 2p XPS spectrum shows two peaks located at 780.1 and 795.8 eV corresponding to the Co²⁺ 2p^{3/2} and 2p^{1/2} the binding energies and another two satellite peaks. The binding energies for Fe³⁺ 2p^{3/2} and 2p^{1/2} are observed at 711.0 and 724.5 eV in agreement with relevant reports.¹

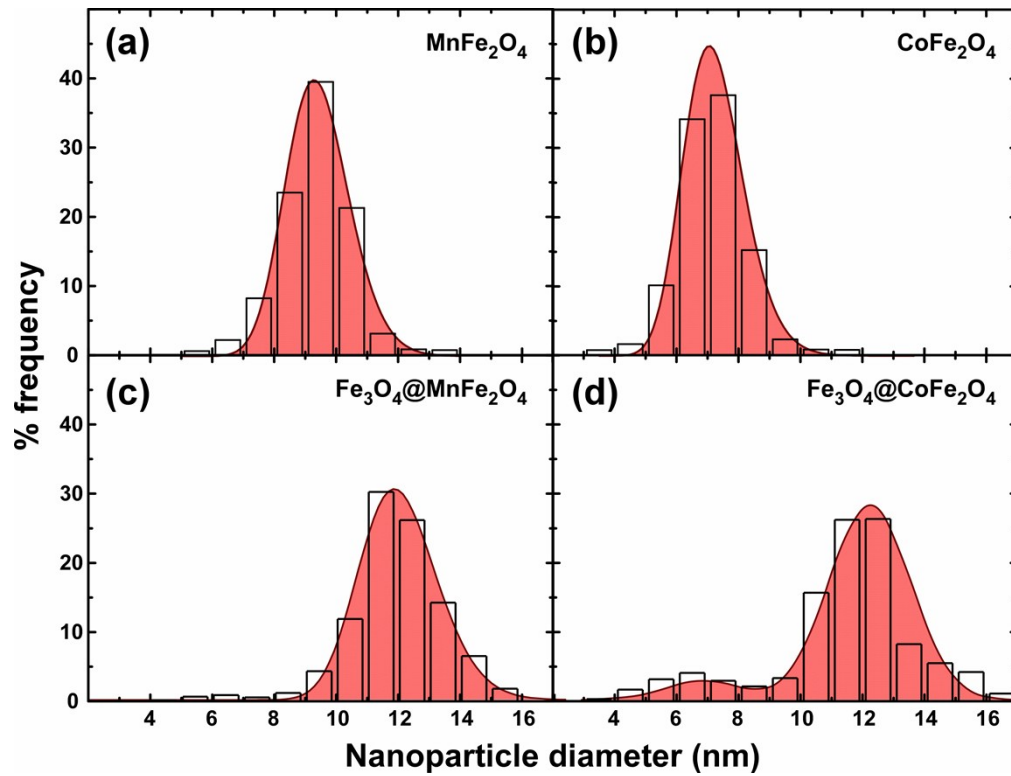


Fig. S2. Size distributions of ferrite-based nanoparticles measured from bright-field TEM images and fitted by lognormal functions. Single phase particles: (a) MnFe_2O_4 and (b) CoFe_2O_4 . Core-shell nanoparticles: (c) $\text{Fe}_3\text{O}_4@\text{MnFe}_2\text{O}_4$, and (d) $\text{Fe}_3\text{O}_4@\text{CoFe}_2\text{O}_4$.

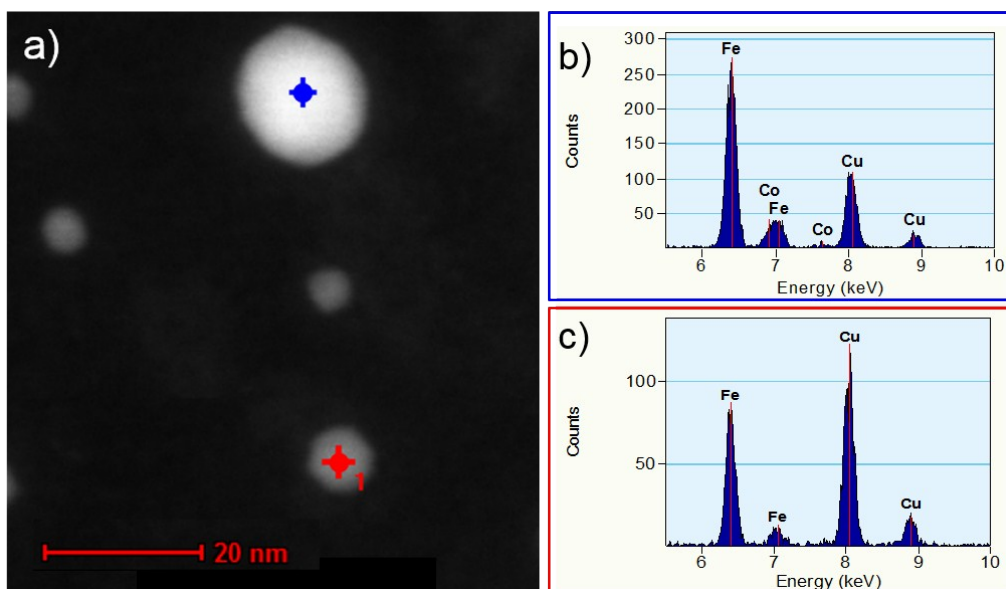


Fig. S3. (a) HAADF/STEM image of magnetite coated CoFe_2O_4 sample. EDX point spectra were taken from a large (b) and a small (c) nanoparticle. The red and blue crosshairs indicate the position of the electron beam for EDX spectroscopy. The large particle contains Fe and Co while the small particle is composed of pure iron oxide within the detection limit. The Cu signal in the spectra originates from the supporting TEM grid.

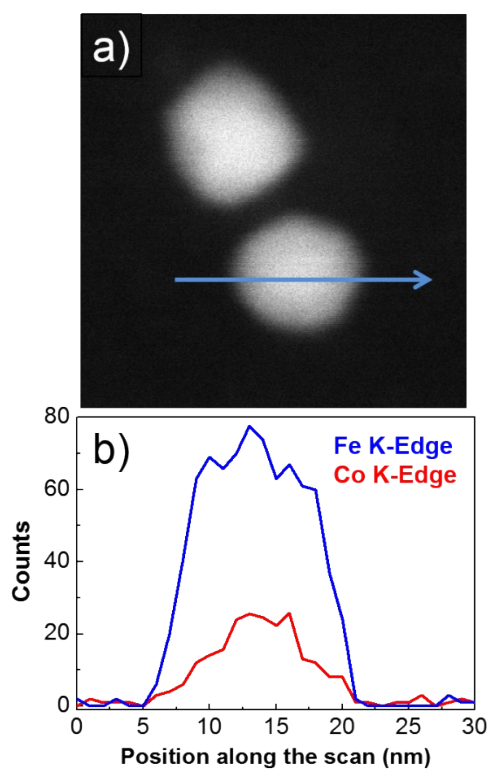


Fig. S4. (a) Representative High Angle Annular Dark Field Scanning TEM (HAADF/STEM) image of the $\text{Fe}_3\text{O}_4@\text{CoFe}_2\text{O}_4$ particles. (b) Elemental profiles of Fe and Co extracted from the line-scan energy dispersive x-ray spectroscopy in the STEM mode along the blue arrow in (a).

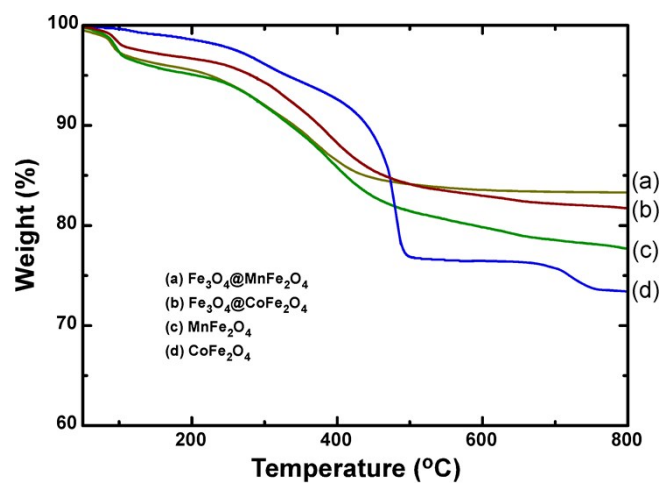


Fig. S5. Thermogravimetric analysis (TGA) curves for samples under study used for normalizing magnetization values.

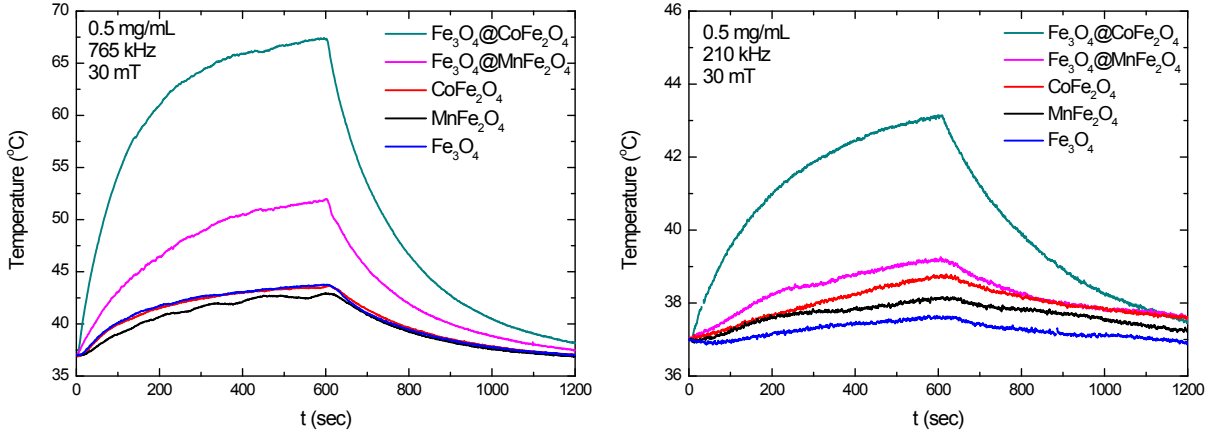


Fig. S6: Hyperthermia cycles of samples under study. Single-phase magnetite particles synthesized under similar conditions are also shown as reference. Left figure corresponds to high frequency (765 kHz) measurement while right to low frequency of 210 kHz. Corresponding SLP values are shown in manuscript's Fig. 6.

The hyperthermia effect is quantified by estimating the specific loss power index (SLP), which refers to the amount of energy converted into heat (J) per time (Δt) and mass of the magnetic material:²

$$SLP = C_p \frac{m_f}{m_{Fe}} \frac{\Delta T}{\Delta t}$$

where C_p is the specific heat of the solution, m_f is the solution mass and $\Delta T/\Delta t$ the initial slope of the heating curve under magnetic field extracted from experimental data (shown in Fig. S4), before the effect of heat conduction becomes important.³

In order to extract a more accurate SLP value, we perform a rigorous data protocol to safely isolate the magnetic-origin heating effect. As shown in our previous works,^{4,5} the experimental curves, where thermal losses occur naturally due to the lower surrounding temperature, are substantially different from the ideal ones (under adiabatic conditions) corresponding to zero thermal losses excluding environmental heat exchanges occurring during measurements. Thus SLP values may appear overestimated and not directly connected with the heating effect of magnetic nanoparticles incorporated. Prior to SLP estimation (i.e. the $\Delta T/\Delta t$ slope evaluation from experimental curves) we perform a two-step routine data process to avoid overestimations and misinterpretations of magnetic nanoparticles heating efficiency as follows:

Step 1-Coil heating effect: Heating of the coil surface becomes pronounced and may lead to misinterpretation (despite cooling water circulating through the copper coil). A gradual increase in the temperature of the coil surface may influence the measurement considerably, despite use of an internal insulating spiral coil and Teflon sample tube. For this reason, a background signal

measured for pure (no MNPs) solution solvent under similar conditions is routinely measured and is subtracted from experimental data to eliminate any contribution to sample temperature from coil heating. This signal may not differ much with field, but its contribution to the overall signal differs substantially based on the overall temperature rise. Therefore, this procedure may lead to considerable changes of the overall signal depending on its relative magnitude. This correction is very important for measurements with low temperature rises, *i.e.*, small sample volumes and/or low solution concentrations, where a small nanoparticle effect may be overestimated because of external heating and misinterpretation of the parameters of Magnetic Particle Hyperthermia.⁶

Step 2-Environmental losses: Following the modified law of cooling,^{5,6} an ideal heating curve is extracted based on fitting of the natural cooling occurring naturally throughout the experimental procedure. By exponentially fitting the cooling stage of the experimental curve (after the AC magnetic field is stopped for $t > 600$ s in Fig. S4), we can estimate the cooling constant and therefore the actual temperature rise after removing heat exchange between sample and environment. The ideal heating curve provides the actual temperature rise caused by the magnetic field of the nanoparticles alone, to increase the accuracy of subsequent SLP estimation by excluding additional heating contributions.

¹ L. Lu, Q. Hao, W. Lei, X. Xia, P. Liu, D. Sun, X. Wang, X. Yang, *Small* 2015, **11** 5833-43.

² L.-Y. Zhang, H.C. Gu, X.-M. Wang, *J. Magn. Magn. Mater.* 2007, **311** 228.

³ T. Samaras, P. Regli and N. Kuster, *Phys. Med. Biol.* 2000, **45** 2233.

⁴ A. Chalkidou, K. Simeonidis, M. Angelakeris, T. Samaras, C. Martinez-Boubeta, Ll. Balcells, K. Papazisis, C. Dendrinou-Samara and O. Kalogirou, *J. Magn. Magn. Mater.*, 2011, **323** 775.

⁵ K. Simeonidis, C. Martinez-Boubeta, Ll. Balcells, C. Monty, G. Stavropoulos, M. Mitrakas, A. Matsakidou, G. Vourlias and M. Angelakeris, *J. Appl. Phys.*, 2013, **114** (10) 103904.

⁶ S. Huang, S.-Y. Wang, A. Gupta, D.-A. Borca-Tasciuc and S. J. Salon, *Measur. Sci. Technol.* 2012, **23**, 035701.